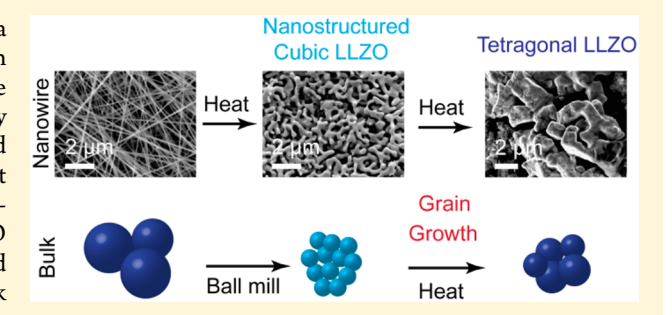
Nanostructured Garnet-Type Solid Electrolytes for Lithium Batteries: Electrospinning Synthesis of Li₇La₃Zr₂O₁₂ Nanowires and Particle Size-Dependent Phase Transformation

Ting Yang, Zachary D. Gordon, Ying Li, and Candace K. Chan*

Materials Science and Engineering, School for Engineering of Matter, Transport and Energy, Arizona State University, 501 E Tyler Mall, ECG 301, Tempe, Arizona 85287, United States

Supporting Information

ABSTRACT: Lithium lanthanum zirconate (LLZO) is a promising ceramic solid electrolyte for all-solid-state lithium batteries with improved safety characteristics. However, the different phases of LLZO differ in lithium ionic conductivity by several orders of magnitude, with extrinsic dopants often required to stabilize the high conductivity cubic phase. Here we show that cubic LLZO can be stabilized at room temperature in nanostructured particles without the use of extrinsic dopants. LLZO nanowires were synthesized using electrospinning and formed cubic phase materials after only 3 h calcination at 700 °C. Bulk LLZO with tetragonal structure was transformed to the cubic



phase using particle size reduction via ball milling. Heating conditions that promoted particle coalescence and grain growth induced a transformation from the cubic to tetragonal phases in both types of nanostructured LLZO. Detailed structural characterizations with XRD and TEM were performed to understand the LLZO formation processes and phase transformations. This work demonstrates another strategy, namely the use of nanostructuring, as an alternative to extrinsic doping for obtaining cubic phase LLZO.

INTRODUCTION

Lithium ion conducting solid electrolytes have great potential for improving the safety characteristics of Li ion batteries. Among the solid-state ceramic electrolytes, the garnet family of materials, $\text{Li}_x\text{La}_3\text{M}_2\text{O}_{12}$ (M = Ta, Nb, Zr), has attracted great interest recently, with Li₇La₃Zr₂O₁₂ (LLZO) emerging as one of the most promising candidates due to its chemical stability in contact with Li metal² and high ionic conductivity.³ Several recent studies investigating the phase stability of LLZO have identified three distinct polymorphs. The first is a hightemperature cubic phase (HT-cubic) that cannot be quenched.⁴⁻⁶ In this structure (c-LLZO, space group $Ia\overline{3}d$, Figure 1a), the Li sublattice is disordered with partial site occupation,⁵ which gives rise to the Li⁺ ionic conductivity on the order of 10⁻⁴ S/cm at room temperature.³ A major drawback to the HT-cubic phase is that it requires hightemperature solid state reaction (>1125 °C) and is not stable at room temperature. Instead, below 650 °C,6 the material transforms into the second phase, which has a tetragonal structure (t-LLZO, space group I4₁/acd, Figure 1b) and ionic conductivity 2-3 orders of magnitude lower than the HT-cubic phase.⁷ The tetragonal distortion is a result of Li⁺ ordering (blue spheres in Figure 1b) that eliminates the short Li-Li interactions and disordered Li⁺ clustering that is responsible for the high conductivity in the HT-cubic phase. 4,8-11 Through the development of low-temperature synthesis methods for LLZO, a third phase with cubic structure has emerged. 12,13 This so-

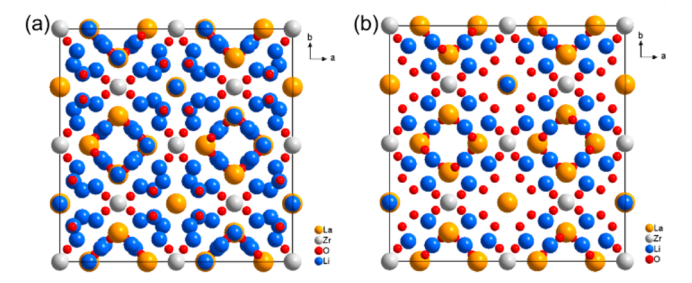


Figure 1. (a) Unit cell of high-temperature cubic phase LLZO, in which clusters of disordered Li ions can be seen. (b) Unit cell of tetragonal phase LLZO. Li ions are ordered and well-separated. Structures plotted from data provided in refs 5 and 7, respectively.

called low-temperature cubic phase (LT-cubic) has the same structure as HT-cubic, but with a slightly larger lattice constant and lower ionic conductivity than even t-LLZO.14 Detailed studies on LT-cubic LLZO have indicated that it may be stabilized at low temperatures due to adsorption of CO₂ or $H_2O^{6,14,15}$ and that it transforms to t-LLZO once these adsorbates are removed using calcination (e.g., between 450 and 650 °C).6

Received: April 14, 2015 Revised: June 11, 2015 Published: June 15, 2015

The Journal of Physical Chemistry C

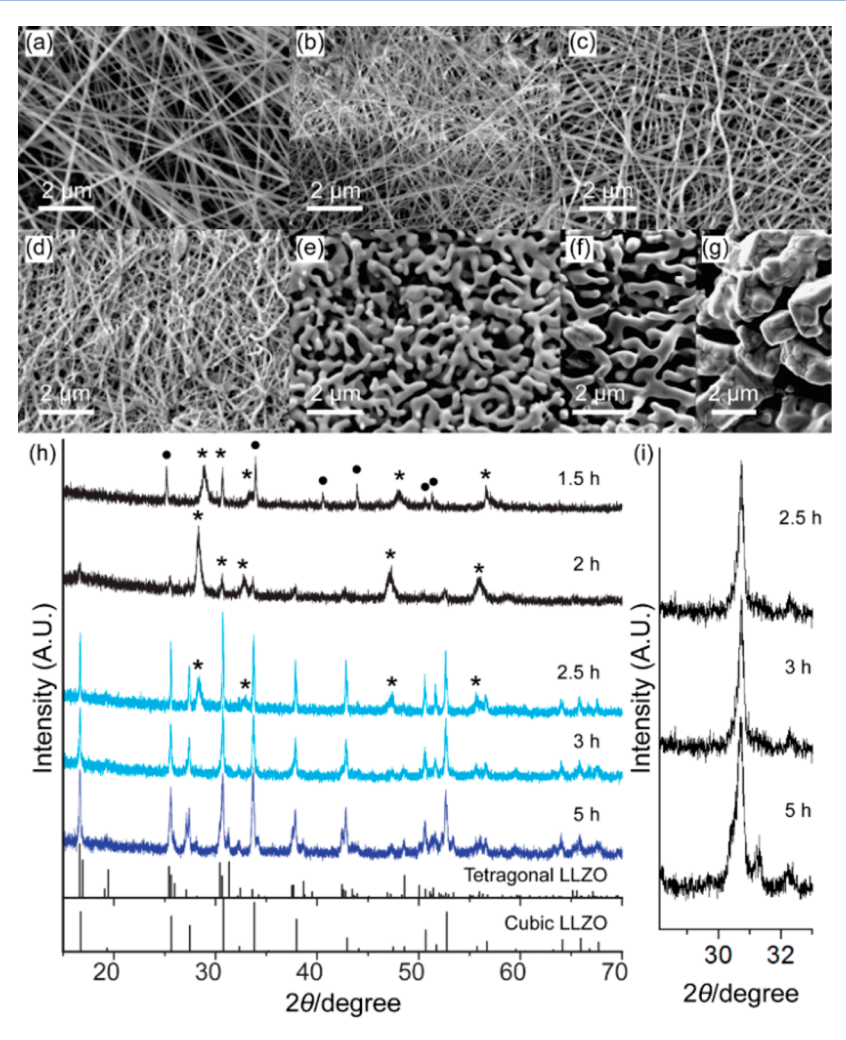


Figure 2. SEM image of (a) as-spun LLZO nanowires and the nanowires after calcination at 700 °C for (b) 1.5, (c) 2, (d) 2.5, (e) 3, and (f, g) 5 h. (h) XRD patterns showing the effect of calcination time on the product: (\bullet) unidentified intermediate phase; (*) La₂Zr₂O₇; (light blue) c-LLZO phase; (dark blue) mixture of tetragonal + cubic LLZO phase. (i) Zoom-in of XRD patterns around 31°, showing the emergence of peak doublet during heating from 2.5 to 5 h. Reference patterns for tetragonal and cubic (with Al doping) LLZO were obtained from the structures provided in refs 5 and 7, respectively.

As it is the phase with the highest ionic conductivity, there is much interest in the HT-cubic structure of LLZO. A number of dopants for stabilizing HT-cubic LLZO at room temperature have been found, such as Al (first introduced inadvertently from Al₂O₃ crucibles during sintering⁵) or Zr substitution by Ta or Nb. 16,17 The stabilization mechanism of Al is believed to be due to the formation of Li⁺ vacancies (2 per each Al³⁺ added to maintain electroneutrality), which increases the total entropy and reduces the free energy gain from Li ordering to destabilize t-LLZO with respect to c-LLZO.9 Indeed, when the Li content is increased from 6.24 to 7.32 per formula unit, a transformation form HT-cubic to t-LLZO was observed. 18 However, the drawback to Al doping is that nonconducting compounds such as LaAlO3 may form as byproducts that segregate at the grain boundaries and are detrimental to the ionic conductivity. 5,19 Also, a higher activation energy for ionic conduction of Li was observed in Al-containing HT-cubic LLZO compared to the Al-free counterpart, likely because the partial occupation of Al on the Li sites can cause increased electrostatic repulsion from the +3 charge of Al and also hinder Li⁺ mobility. ⁶ For Zr substitutional dopants such as Ta and Nb, a narrow composition range for peak conductivity was observed, meaning the doping must be carefully controlled. 17,20,21

Hence, it is advantageous to find other ways to stabilize the HT-cubic LLZO phase at room temperature without relying on extrinsic dopants.

Herein we report our observations on a phenomenon that has not been fully discussed before, namely the size-dependent transformations and phase stability in LLZO. We show that c-LLZO can be stabilized at room temperature in nanostructured particles without the use of extrinsic dopants and that heating to promote coalescence and grain growth causes a transformation to t-LLZO. As several recent studies have shown advantages of nanostructured LLZO (such as higher ionic conductivity, ²² cycling performance and current density, ¹⁹ and fracture strength ²³) compared to bulk LLZO, improved understanding of this size-dependent phase change may be important for the development of better LLZO-based electrolytes for safer Li-ion batteries.

EXPERIMENTAL METHODS

In order to obtain nanostructured LLZO and investigate its phase transformations, the electrospinning technique was selected as it has been a versatile method for preparing ceramic nanofibers or nanowires from sol–gel precursors. ^{24,25} To our

knowledge, this is the first report of the synthesis of LLZO nanowires using electrospinning. The synthesis of LLZO nanowires also enables detailed structural characterization using transmission electron microscopy (TEM) to better understand the formation mechanism of LLZO synthesized from sol-gel precursors.

The electrospinning precursor for the LLZO nanowires was prepared by mixing either a nitrate or acetate based sol into a polyvinylpyrrolidone (PVP) solution (Supporting Information). After electrospinning, the as-spun nanowires were peeled off the collector as a flexible mat (Figure S1) and calcined in an alumina crucible in air at 700 °C to remove the PVP and crystallize the nanowires. The nanowires prepared with both types of sol precursors gave similar morphology and crystal structures. However, the LLZO nanowires prepared with nitrate precursors tended to have more byproducts (Figure S1d). Bulk LLZO was prepared using the sol-gel method described by Janani et al. but without the addition of Al₂O₃. A photograph of an as-spun flexible nanowire mat is shown in Figure S1a.

■ RESULTS AND DISCUSSION

Scanning electron microscope (SEM) images of the as-spun nanowires prepared from acetate precursors are shown in Figure 2a, showing diameters ranging from ~100 to 200 nm. Figure 2b-e shows the morphology evolution of the LLZO nanowires after being heated at 700 °C for 1.5, 2, 2.5, and 3 h, respectively. Figures 2f and 2g are both from the same sample that was calcined for 5 h. The dimensions and morphology of the nanowires did not change much after 1.5 h of heating (Figure 2b). However, as the heating time increased, the nanowires became thicker and underwent coalescence to form larger ligaments. More interestingly, these morphology changes were also accompanied by a phase transformation, as determined using X-ray diffraction (XRD). As shown in Figure 2h, 1.5 h was not sufficient time for formation of LLZO. The peaks labeled with asterisks belong to the intermediate phase La₂Zr₂O₇. After 2 h of calcination, a small amount of cubic phase LLZO was observed, but the majority of the sample was still La₂Zr₂O₇. After calcination for 2.5 h, c-LLZO was the majority product, and the amount of La₂Zr₂O₇ decreased significantly. This is also consistent with the findings of other groups that La₂Zr₂O₇ is the first intermediate phase as well as the main byproduct. 3,12,13,23

To better understand the spatial distribution of La₂Zr₂O₇ and LLZO in the nanowire sample calcined for 2.5 h, TEM studies were performed. As shown in Figure 3, TEM imaging revealed that the sample contained two types of morphologies. Polycrystalline nanowires composed of small crystallites 10 to 20 nm in size (Figure 3a, inset) were observed as the first morphology. The measured lattice spacing from the highresolution TEM (HRTEM) image is 3.12 Å (Figure 3b, inset), which corresponds to the {222} spacing of La₂Zr₂O₇. It is also evident from the corresponding XRD pattern (Figure 2h, 2.5 h) that the La₂Zr₂O₇ peaks are broadened, indicating nanosized crystallites. The nanowires appeared to be surrounded by a layer of amorphous material, as noted by the arrows in Figure 3b, which is believed to be a Li-containing amorphous phase. The formation of sol-gel derived LLZO from La₂Zr₂O₇ and an amorphous Li-phase has been proposed before 23 based on XRD analysis. Figure 3c shows the other morphology, which is composed of much larger crystals with particle size of 100-200 nm interconnected to form ligaments, similar to those observed

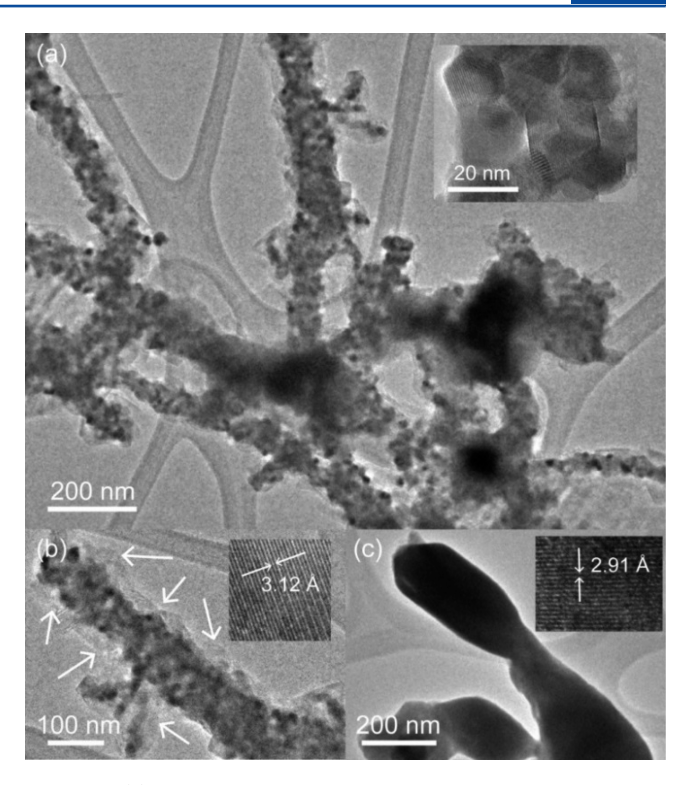


Figure 3. (a) TEM image of the sample calcined for 2.5 h, showing one of the morphologies. Inset is a zoomed-in view showing the La₂Zr₂O₇ crystals. (b) TEM image of one branch in (a). Areas indicated by arrows are considered to be Li-containing amorphous phase. Inset is an HRTEM image showing the lattice fringes. (c) TEM image of the sample calcined for 2.5 h, showing the other morphology (LLZO crystals). Inset shows the HRTEM image with lattice fringes.

more distinctly in the SEM images of the samples calcined for 3 h (Figure 2e). The inset in Figure 3c is a HRTEM image showing the lattice fringes with d = 2.91 Å, in good agreement with the {024} spacing (2.90 Å) in c-LLZO. Because of the thickness of the samples, it was difficult to measure the grain sizes within the ligaments, but using the Scherrer equation on the XRD pattern revealed a grain size of ~65 nm, which is smaller than the size of the ligament diameter.

From the image in Figure 3a, it appears that nucleation of these ligaments occurs at intersections between adjacent or crossing nanowires, as shown by the dark regions. These results along with the XRD data in Figure 2h suggest that during the calcination process, La₂Zr₂O₇ first forms as small crystallites within the nanowire core and then reacts with the amorphous, Li-rich shell to form c-LLZO. During the reaction, the nanowires change in morphology, and the resulting c-LLZO forms ligaments with larger grain sizes due to the coalescence of neighboring La₂Zr₂O₇ crystallites with the amorphous Licontaining regions. To our knowledge, this is the first time that the formation steps of LLZO are revealed, which is made possible by studying the LLZO nanowires synthesized by electrospinning.

As shown in the XRD pattern in Figure 2h, after 3 h of calcination, the sample was composed of phase pure c-LLZO, which is consistent with the SEM images showing the sample morphology consisted entirely of ligaments associated with c-LLZO. The c-LLZO derived from the electrospun nanowires was structurally stable, as XRD performed on a sample after 14 months of storage showed the structure remained in the cubic phase (Figure S2). When heated for an additional 2 h, some of

the XRD peaks split into "doublets" (Figure 2h, 5 h), which indicates the emergence of t-LLZO. This is shown more clearly in Figure 2i, in which the (024) planes for cubic LLZO split into the tetragonal double peaks as the set of (042) and (024) at $\sim 31^{\circ}$. Based on the visible coarsening of grains from the corresponding SEM images in Figures 2f and 2g, this cubic to tetragonal phase transformation between 3 and 5 h calcination time appears to be due to the increase in ligament diameter. Morphologically, the 5 h sample is a mixture of small ligaments (Figure 2f) and larger micron-sized particles (Figure 2g). The small ligaments are almost identical in morphology and size to the ones observed in the 3 h sample. Therefore, it is not unreasonable to assign the c-LLZO peaks to the small ligaments. On the other hand, the large particles would give rise to the tetragonal peaks emerging in the XRD pattern. Hence, from these results, we can see a clear correlation between the particle size and preferred crystal structure, with smaller particles adopting the cubic phase and larger particles the tetragonal phase.

In fact, similar observations have been made in other studies. Kokal et al. synthesized Al-free LLZO using a Pechini sol-gel method and calcined the sample at various temperatures. They found that after heating at 700 °C, the sample was c-LLZO with a particle size of 300-500 nm. When 800 °C was used, the particle size increased to 500-1000 nm and the phase changed to tetragonal.¹² In the study by Xie et al., Al-free cubic phase LLZO ~20 nm in size was also obtained with sol-gel methods.²⁶ Neither of the aforementioned groups discussed the possible mechanism for stabilization of the cubic phase in Al-free LLZO. Several mechanisms from the literature could be in play e.g. a high concentration of Li vacancies, 9,18,27 $\rm CO_2$ adsorption, 6,14 and $\rm H_2O$ doping 15 (the latter two which are proposed to stabilize the LT-cubic phase). Additionally, here we propose another possible mechanism, in which the phase transformation can be induced by the change in particle size as a result of the difference in surface energy between the cubic and tetragonal LLZO phases.

Several differential thermal analysis (DTA) and differential scanning calorimetry (DSC) studies have shown that the t-LLZO to HT-cubic phase transformation is an endothermic reaction and the reverse transformation is an exothermic one. 6,12,15 Filipovich, Kalinina, and Garvie independently postulated that for any solid state endothermic transformation, there exists a critical crystallite size below which the hightemperature structure is stable at temperatures much lower than the bulk transformation temperature. 28,29 This in fact has been confirmed both theoretically and experimentally in several systems, perhaps most famously in the titania (TiO₂) and zirconia (ZrO₂) polymorphs. At room temperature, bulk titania is only stable in the rutile phase, but the anatase phase can exist when the crystallite size is reduced to a few nanometers.^{30–32} For zirconia, the monoclinic structure is the stable phase at room temperature, and it transforms to a tetragonal phase at around 1200 °C. 29,33 Since pure zirconia cannot be quenched to retain the tetragonal phase, a common practice is to stabilize it with dopants such as yttria (Y2O3) to form yttria-stabilized zirconia (YSZ). However, by reducing the size of the crystals, the tetragonal phase can exist at ambient conditions without requiring extrinsic dopants. 25,29,33-35 The origin of this phenomenon is the difference in surface energy between the two polymorphs for each material. As proposed by Garvie,²⁹ the most probable reason for such a transformation is that the high-temperature phase zirconia has a lower surface energy

than the low-temperature phase. When the crystallite size is sufficiently small, the material has to undergo a phase transformation to the low surface energy phase in order to relieve the internal stress. Indeed, it was verified that the surface energy of rutile is larger than that of anatase, ³⁰ and the surface energy of monoclinic zirconia is larger than that of tetragonal zirconia. ³⁴ On the basis of this previous work, therefore, we envision that a similar size-dependent phase transformation could also be present in LLZO. In other words, for particles with grains below a critical size, the HT-cubic phase of LLZO will be more stable than the t-LLZO phase at room temperature.

Several proof-of-concept experiments were conducted as followed. First, bulk LLZO powder was prepared and calcined at 700 °C for 3 h in an alumina crucible. Unlike the electrospun nanowires, these conditions were not sufficient for complete phase transformation, as the products were a mixture of the cubic and tetragonal phases (Figure S3). This shows that the shorter diffusion distances for the reactants (e.g., diffusion of Li from the Li-rich amorphous phase) in the nanowires is advantageous for obtaining the crystallized LLZO using shorter calcination times. After calcining the bulk LLZO at 700 °C for 5 h, the XRD pattern showed the product was t-LLZO (Figure 4a). SEM imaging of this product showed agglomerated

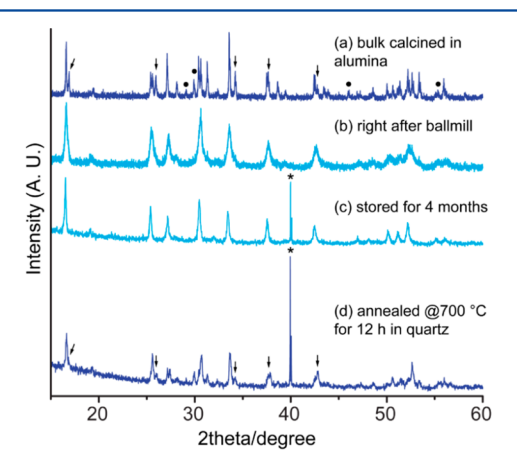


Figure 4. XRD patterns of bulk LLZO prepared from nitrate sol-gel (a) after calcining at 700 °C for 5 h, (b) after ball milling, (c) after storage for 4 months, and (d) after annealing at 700 °C for 12 h. The bulk LLZO changed from tetragonal to cubic after ball milling with the re-emergence of t-LLZO after heating. Tetragonal peak doublets are marked with arrows. Dark blue: t-LLZO; light blue: c-LLZO; ●: La_2O_3 ; *: unknown contaminants/byproduct.

particles 1–10 μ m in size (Figure S4a). These results are consistent with the calcination studies on the c-LLZO nanowires showing that the t-LLZO structure was favored for the larger particle sizes. The data also show that Al dopant diffusion from the crucible was unlikely in the calcination conditions used, which rules out the possibility that stabilization of c-LLZO in the nanowires calcined at 700 °C for 3 h was from Al dopants. Example reaction conditions that have been used to intentionally introduce Al dopants include 850 °C for 25 h³⁶ or 1180 °C for 35 h.^{37,38} Moreover, examination using energy dispersive X-ray spectroscopy (EDX) in the SEM showed that there was no Al in the c-LLZO nanowire sample (Figure S5). Calcination of the as-spun nanowires in a quartz crucible at 700 °C for 3 h also resulted in the c-LLZO structures (Figure S1d), further suggesting that the stabilization

is due to the small size of the nanowires and not from Al

The bulk t-LLZO was then subjected to ball milling for 1 h in order to reduce the particles sizes. SEM imaging after ball milling showed that the sample consisted of agglomerates of smaller particles (Figure S4b). The XRD pattern (Figure 4b) of the ball milled sample showed broadening of the diffraction peaks, which is an indication of particle size reduction. The grain size was determined to be ~25 nm using the Scherrer equation. Additionally, most of the tetragonal double peaks became unified, indicating the transformation of the bulk t-LLZO to c-LLZO after ball milling. The ball milled powder was then stored in a capped scintillation vial in air. After 4 months, the sample was re-examined with XRD. Notably, the ball-milled sample was still c-LLZO (Figure 4c); also, the peak widths had significantly reduced, and the position of some peaks had shifted, which we interpret to be due to the relaxation of the large residual strain induced by ball milling. This stored sample was then annealed at 700 °C in a quartz crucible for 12 h, the same temperature at which the sample was initially synthesized, to induce grain growth. The resulting XRD pattern (Figure 4d) showed that a number of the doublets reappeared, indicating the return of t-LLZO. According to the Scherrer equation, the grain size of the c-LLZO doubled to ~50 nm, and the grains corresponding to the t-LLZO peaks were even larger at ~80 nm. This further confirms our hypothesis that c-LLZO can be stabilized below a certain critical grain size and that transformation to t-LLZO during heating is due to grain growth and particle coalescence. This notion that c-LLZO can exist at room temperature without stabilizing extrinsic dopants provided the particle size is small enough is consistent with our results as well as those reported by Kokal et al. 12 and Xie et al. 26 We point out that the recent work by Teng et al.,³⁹ whereby t-LLZO was transformed to c-LLZO using pulsed laser annealing, is not in conflict with our observations, as the LLZO grain sizes in that work were \sim 4 μ m, and the laser irradiation may have caused sufficient local heating to thermally promote the tetragonal to cubic phase transformation.

On the other hand, the fact that the LT-cubic phase is difficult to distinguish from the HT-cubic phase by XRD complicates the discussion. One could argue that since smaller particles have larger surface area, the stabilization effect from adsorption of CO₂/H₂O would be easier than with larger particles. For example, as shown by Toda et al., t-LLZO (presumably bulk particles, although the size was not reported) transformed into the LT-cubic phase after being annealed in air at 450 °C for 20 h. Partial transformation back to t-LLZO could be achieved with heating at temperatures as low as 600 °C to drive off the CO2; full transformation could be achieved by annealing at 800 °C for just 1 h. 14 Matsui et al. also showed that the extraction of CO₂ from LLZO occurs around 450–650 °C.6 On the basis of these results, we believe that calcination of LTcubic LLZO at 700 °C for 12 h would most likely drive off any adsorbed CO2 or H2O and cause the material to transform completely to t-LLZO, if the cubic phase stabilization were indeed adsorption-based. Since our sample remained mostly c-LLZO (Figure 4d), it is not likely that the stabilization was, as reported for the LT-cubic phase, due to CO2 or H2O adsorption. Similarly, in Xie et al.'s study, their cubic phase LLZO had been calcined at 750 °C for 20 h, 26 which means that it is also unlikely that CO2 or H2O was causing the stabilization. Since in their study detailed particle size information was not provided, it is not clear how much

coalescence had occurred after 20 h of calcination. From the TEM data provided, the LLZO was still only 20 nm after 8 h of calcination at 750 °C, so the crystallite size could still be smaller than the critical transition size even after 20 h of calcination.

This critical grain size for the LLZO phase transition can be determined from the difference in surface energy between the cubic and tetragonal phases. In the titania and zirconia systems, the calculated critical grain size showed good agreement to the experimental observations.^{32,34} The surface energy difference between rutile and anatase titania is approximately 0.59 J/m², and the critical size is \sim 14 nm. ³² For monoclinic and tetragonal zirconia, the surface energy difference is ~0.36 J/m² and the critical size is ~9 nm.34 Hence, we can see that a smaller difference in the surface energy between the two structures would require a smaller critical grain size in order to stabilize the higher temperature phase. Although the surface energy for the tetragonal and cubic LLZO structures is not yet known, we expect that the surface energy difference is relatively large, since the LLZO grains must be at least larger than the La₂Zr₂O₇ crystallites. On the basis of our SEM and TEM data, it appears that c-LLZO with dimensions of ~200 nm (the grain size would be even smaller, since the LLZO studied here was polycrystalline) have sufficient excess surface area to be stabilized at room temperature, which can be feasibly obtained with top-down approaches such as ball milling in addition to more sophisticated chemical synthesis approaches such as the electrospinning method we present here.

While achieving c-LLZO particles using these surface energy considerations should not be difficult, the more challenging aspect is how to maintain the cubic phase once it is integrated into a suitable form, such as a dense pellet, for use as a solid state electrolyte in a Li ion battery. Conventional sintering conditions for preparing dense LLZO pellets, e.g. calcination at 1230 °C for 36 h, would encourage significant grain growth/ coalescence and hence transformation of the c-LLZO to t-LLZO. Ionic conductivity measurements on pellets derived from Al-free, c-LLZO fine powders synthesized using sol-gel methods at 750-800 °C gave rather low bulk conductivities $\sim 10^{-6} \text{ S/cm}^{14,26}$ or 2 orders of magnitude lower than the c-LLZO stabilized with Al doping at high temperature. This is why the LT-cubic phase was proposed as a separate (and undesired) polymorph of LLZO with low ionic conductivity. However, on the basis of the observations presented here, it is possible that this low apparent ionic conductivity is due to the c-LLZO transformation to the tetragonal phase during the pellet formation. For this reason, structural characterization of fine powders should be performed after densification, particularly for correlation to ionic conductivity measurements.

Another possible reason for the lower ionic conductivity observed in Al-free, nanostructured c-LLZO could be a high grain boundary resistance in the sintered pellet due to insufficient densification.¹⁴ Wolfenstine et al. found that the total conductivity of tetragonal phase LLZO can be greatly improved by about 2 orders of magnitude to $\sim 10^{-5}$ S/cm by making a very dense pellet (~98% relative density) through hot-pressing. 40 Nanoparticles have very large surface-to-volume ratios and should in theory yield sintered pellets with high density but tend to form agglomerates due to electrostatic or van der Waals forces. Indeed, we observed this phenomenon in the ball-milled LLZO (Figure S4b). Particles are more closepacked within each agglomerate, but the interagglomerate pores are large. 41-44 During sintering, these agglomerates can reach near-full density, while the pores between them are difficult to eliminate. This is because that the surface energy of the assintered agglomerate is already significantly reduced, and hence the material loses its driving force to densify further. This could possibly explain the high grain boundary resistivity observed in the c-LLZO pellets prepared by Xie et al., which had a density of only 89.2%.²⁶

In this regard, the electrospun LLZO nanowires have a clear advantage in that nanocrystallites connect to each other and form larger structures (nanowires) at the crystallization stage. Thus, agglomeration in nanopowders derived from electrospinning can be greatly prevented while maintaining many high energy surfaces, which means the main driving force for sintering is not compromised. Additionally, advanced sintering techniques such as two-step sintering (TSS), spark plasma sintering (SPS), or templated grain growth sintering (TGGS) may also be employed to create dense pellets from c-LLZO nanowires. TSS suppresses grain growth by first using ratecontrolled sintering to produce uniform pore microstructures followed by sintering at a lower temperature where grain boundary-controlled densification predominates.⁴⁵ SPS uses a very high current through the material, causing localized heating, with pressure supplied at the same time. Therefore, the temperature required is much lower than conventional sintering and grain growth is greatly inhibited. 46 TGGS is typically achieved by embedding anisotropic particles into a precursor matrix, followed by calcination to grow the templates from the matrix materials and densify the films.⁴⁷ All of these methods have been used for preparing dense pellets of other types of nanowires while preserving the 1D morphologies 45-49 and are anticipated to work similarly for LLZO nanowires. Moreover, the highly anisotropic nanowires are ideal templates for using TGGS to obtain dense films.

CONCLUSIONS

In summary, we synthesized LLZO nanowires with electrospinning for the first time. During calcination, $\rm La_2Zr_2O_7$ nanocrystals and Li-containing amorphous phases are first formed and then react with further annealing time to form c-LLZO. We also show that the transformation between the tetragonal and cubic phases in the LLZO system can be induced by a change in dimensions, with c-LLZO stabilized in nanostructures and t-LLZO preferred for larger particles. The mechanism is likely related to the difference in surface energy between the high-temperature cubic phase and the low-temperature tetragonal phase. Using nanostructured LLZO as solid electrolyte can be beneficial in terms of ionic conductivity, cycle life, and mechanical strength, in addition to improving the safety characteristics of lithium ion batteries.

ASSOCIATED CONTENT

Supporting Information

Experimental methods and characterization details; SEM and XRD of LLZO nanowires prepared by electrospinning from nitrate precursors; XRD of bulk LLZO after calcination at 700 °C for 3 h; XRD of c-LLZO after long-term storage; SEM of bulk LLZO; EDX spectrum of c-LLZO nanowires. The Supporting Information is available free of charge on the ACS Publications website at DOI: 10.1021/acs.jpcc.5b03589.

AUTHOR INFORMATION

Corresponding Author

*E-mail candace.chan@asu.edu; phone (480) 727-8614 (C.K.C.).

Notes

The authors declare no competing financial interest.

ACKNOWLEDGMENTS

This work was supported by new faculty startup funds from the Fulton Schools of Engineering at ASU as well as funding from NSF DMR-1206795. Z.D.G. thanks the Fulton Undergraduate Research Initiative at ASU for funding. We gratefully acknowledge the use of facilities within the LeRoy Center for Solid State Science and Goldwater Environmental Laboratory at ASU.

REFERENCES

- (1) Thangadurai, V.; Kaack, H.; Weppner, W. J. F. Novel Fast Lithium Ion Conduction in Garnet-Type $\text{Li}_5\text{La}_3\text{M}_2\text{O}_{12}$ (M = Nb, Ta). *J. Am. Ceram. Soc.* **2003**, *86*, 437–440.
- (2) Thangadurai, V.; Adams, S.; Weppner, W. Crystal Structure Revision and Identification of Li⁺-Ion Migration Pathways in the Garnet-like Li₅La₃M₂O₁₂ (M = Nb, Ta) Oxides. *Chem. Mater.* **2004**, *16*, 2998–3006.
- (3) Murugan, R.; Thangadurai, V.; Weppner, W. Fast Lithium Ion Conduction in Garnet-Type Li₇La₃Zr₂O₁₂. *Angew. Chem., Int. Ed.* **2007**, 46, 7778–7781.
- (4) Percival, J.; Kendrick, E.; Smith, R. I.; Slater, P. R. Cation Ordering in Li Containing Garnets: Synthesis and Structural Characterisation of the Tetragonal System, Li₇La₃Sn₂O₁₂. *Dalton Trans.* **2009**, 5177–5181.
- (5) Geiger, C. A.; Alekseev, E.; Lazic, B.; Fisch, M.; Armbruster, T.; Langner, R.; Fechtelkord, M.; Kim, N.; Pettke, T.; Weppner, W. Crystal Chemistry and Stability of "Li₇La₃Zr₂O₁₂" Garnet: A Fast Lithium-Ion Conductor. *Inorg. Chem.* **2011**, *50*, 1089–1097.
- (6) Matsui, M.; Takahashi, K.; Sakamoto, K.; Hirano, A.; Takeda, Y.; Yamamoto, O.; Imanishi, N. Phase Stability of a Garnet-Type Lithium Ion Conductor Li₇La₃Zr₂O₁₂. *Dalton Trans.* **2014**, *43*, 1019–1024.
- (7) Awaka, J.; Kijima, N.; Hayakawa, H.; Akimoto, J. Synthesis and Structure Analysis of Tetragonal Li₇La₃Zr₂O₁₂ with the Garnet-Related Type Structure. *J. Solid State Chem.* **2009**, 182, 2046–2052.
- (8) Cussen, E. J. The Structure of Lithium Garnets: Cation Disorder and Clustering in a New Family of Fast Li⁺ Conductors. *Chem. Commun.* **2006**, 412–413.
- (9) Bernstein, N.; Johannes, M. D.; Hoang, K. Origin of the Structural Phase Transition in Li₇La₃Zr₂O₁₂. *Phys. Rev. Lett.* **2012**, *109*, 205702.
- (10) Jalem, R.; Yamamoto, Y.; Shiiba, H.; Nakayama, M.; Munakata, H.; Kasuga, T.; Kanamura, K. Concerted Migration Mechanism in the Li Ion Dynamics of Garnet-Type $\text{Li}_7\text{La}_3\text{Zr}_2\text{O}_{12}$. Chem. Mater. **2013**, 25, 425–430.
- (11) Meier, K.; Laino, T.; Curioni, A. Solid-State Electrolytes: Revealing the Mechanisms of Li-Ion Conduction in Tetragonal and Cubic LLZO by First-Principles Calculations. *J. Phys. Chem. C* **2014**, *118*, 6668–6679.
- (12) Kokal, I.; Somer, M.; Notten, P. H. L.; Hintzen, H. T. Sol-gel Synthesis and Lithium Ion Conductivity of $\text{Li}_7\text{La}_3\text{Zr}_2\text{O}_{12}$ with Garnet-Related Type Structure. *Solid State Ionics* **2011**, *185*, 42–46.
- (13) Janani, N.; Ramakumar, S.; Dhivya, L.; Deviannapoorani, C.; Saranya, K.; Murugan, R. Synthesis of Cubic Li₇La₃Zr₂O₁₂ by Modified Sol-Gel Process. *Ionics* **2011**, *17*, 575–580.
- (14) Toda, S.; Ishiguro, K.; Shimonishi, Y.; Hirano, A.; Takeda, Y.; Yamamoto, O.; Imanishi, N. Low Temperature Cubic Garnet-Type CO₂-Doped Li₇La₃Zr₂O₁₂. *Solid State Ionics* **2013**, 233, 102–106.
- (15) Larraz, G.; Orera, A.; Sanjuán, M. L. Cubic Phases of Garnet-Type Li₇La₃Zr₂O₁₂: The Role of Hydration. *J. Mater. Chem. A* **2013**, *1*, 11419–11428.
- (16) Logéat, A.; Köhler, T.; Eisele, U.; Stiaszny, B.; Harzer, A.; Tovar, M.; Senyshyn, A.; Ehrenberg, H.; Kozinsky, B. From Order to Disorder: The Structure of Lithium-Conducting Garnets $\operatorname{Li}_{7-x}\operatorname{La}_3\operatorname{Ta}_x\operatorname{Zr}_{2-x}\operatorname{O}_{12}$ (x=0-2). Solid State Ionics 2012, 206, 33–38.

- (17) Ohta, S.; Kobayashi, T.; Asaoka, T. High Lithium Ionic Conductivity in the Garnet-Type Oxide $\text{Li}_{7.X} \, \text{La}_3(\text{Zr}_{2.X}, \, \text{Nb}_X) \, \text{O}_{12} \, (X = 0-2)$. *J. Power Sources* **2011**, *196*, 3342–3345.
- (18) Rangasamy, E.; Wolfenstine, J.; Sakamoto, J. The Role of Al and Li Concentration on the Formation of Cubic Garnet Solid Electrolyte of Nominal Composition Li₇La₃Zr₂O₁₂. Solid State Ionics **2012**, 206, 28–32.
- (19) Cheng, L.; Chen, W.; Kunz, M.; Persson, K.; Tamura, N.; Chen, G.; Doeff, M. Effect of Surface Microstructure on Electrochemical Performance of Garnet Solid Electrolytes. *ACS Appl. Mater. Interfaces* **2015**, *7*, 2073–2081.
- (20) Buschmann, H.; Berendts, S.; Mogwitz, B.; Janek, J. Lithium Metal Electrode Kinetics and Ionic Conductivity of the Solid Lithium Ion Conductors "Li₇La₃Zr₂O₁₂" and Li_{7-x}La₃Zr_{2-x}Ta_xO₁₂ with Garnet-Type Structure. *J. Power Sources* **2012**, 206, 236–244.
- (21) Wang, Y.; Lai, W. High Ionic Conductivity Lithium Garnet Oxides of Li_{7-x}La₃Zr_{2-x}Ta_xO₁₂ Compositions. *Electrochem. Solid-State Lett.* **2012**, *15*, A68–A71.
- (22) Tenhaeff, W. E.; Rangasamy, E.; Wang, Y.; Sokolov, A. P.; Wolfenstine, J.; Sakamoto, J.; Dudney, N. J. Resolving the Grain Boundary and Lattice Impedance of Hot-Pressed Li₇La₃Zr₂O₁₂ Garnet Electrolytes. *ChemElectroChem* **2014**, *1*, 375–378.
- (23) Sakamoto, J.; Rangasamy, E.; Kim, H.; Kim, Y.; Wolfenstine, J. Synthesis of Nano-Scale Fast Ion Conducting Cubic Li₇La₃Zr₂O₁₂. *Nanotechnology* **2013**, *24*, 424005.
- (24) Li, D.; Xia, Y. Fabrication of Titania Nanofibers by Electrospinning. *Nano Lett.* **2003**, *3*, 555–560.
- (25) Davies, E.; Lowe, A.; Sterns, M.; Fujihara, K.; Ramakrishna, S. Phase Morphology in Electrospun Zirconia Microfibers. *J. Am. Ceram. Soc.* **2008**, *91*, 1115–1120.
- (26) Xie, H.; Li, Y.; Goodenough, J. B. Low-Temperature Synthesis of Li₇La₃Zr₂O₁₂ with Cubic Garnet-Type Structure. *Mater. Res. Bull.* **2012**, 47, 1229–1232.
- (27) Thompson, T.; Wolfenstine, J.; Allen, J. L.; Johannes, M.; Huq, A.; David, I. N.; Sakamoto, J. Tetragonal vs. Cubic Phase Stability in Al-Free Ta Doped Li₇La₃Zr₂O₁₂ (LLZO). *J. Mater. Chem. A* **2014**, 2, 13431–13436.
- (28) Filipovich, V. N.; Kalinina, A. M. Critical Amorphization Radius of Crystals. *Struct. Glass* **1965**, *5*, 34.
- (29) Garvie, R. C. Stabilization of the Tetragonal Structure in Zirconia Microcrystals. *J. Phys. Chem.* **1978**, *82*, 218–224.
- (30) Gribb, A. A.; Banfield, J. F. Particle Size Effects on Transformation Kinetics and Phase Stability in Nanocrystalline TiO₂. Am. Mineral. **1997**, 82, 717–728.
- (31) Hu, Y.; Tsai, H.-L.; Huang, C.-L. Phase Transformation of Precipitated TiO₂ Nanoparticles. *Mater. Sci. Eng., A* **2003**, 344, 209–214
- (32) Zhang, H.; Banfield, J. F. Thermodynamic Analysis of Phase Stability of Nanocrystalline Titania. *J. Mater. Chem.* **1998**, *8*, 2073–2076.
- (33) Garvie, R. C. The Occurrence of Metastable Tetragonal Zirconia as a Crystallite Size Effect. *J. Phys. Chem.* **1964**, *69*, 1238–1243.
- (34) Chraska, T.; King, A. H.; Berndt, C. C. On the Size-Dependent Phase Transformation in Nanoparticulate Zirconia. *Mater. Sci. Eng., A* **2000**, *A286*, 169–178.
- (35) Baldinozzi, G.; Simeone, D.; Gosset, D.; Dutheil, M. Neutron Diffraction Study of the Size-Induced Tetragonal to Monoclinic Phase Transition in Zirconia Nanocrystals. *Phys. Rev. Lett.* **2003**, *90*, 216103.
- (36) Hubaud, A. A.; Schroeder, D. J.; Key, B.; Ingram, B. J.; Dogan, F.; Vaughey, J. T. Low Temperature Stabilization of Cubic (Li_{7-x}Al_{x/3})La₃Zr₂O₁₂: Role of Aluminum during Formation. *J. Mater. Chem. A* **2013**, *1*, 8813–8818.
- (37) Kaeriyama, A.; Munakata, H.; Kajihara, K.; Kanamura, K.; Sato, Y.; Yoshida, T. Evaluation of Electrochemical Characteristics of Li₂La₃Zr₂O₁, Solid Electrolyte. *ECS Trans.* **2009**, *16*, 175–180.
- (38) Shimonishi, Y.; Toda, A.; Zhang, T.; Hirano, A.; Imanishi, N.; Yamamoto, O.; Takeda, Y. Synthesis of Garnet-Type Li_{7-x}La₃Zr₂O_{12-1/2x} and Its Stability in Aqueous Solutions. *Solid State Ionics* **2011**, *183*, 48–53.

- (39) Teng, S.; Tan, J.; Tiwari, A. Recent Developments in Garnet Based Solid State Electrolytes for Thin Film Batteries. *Curr. Opin. Solid State Mater. Sci.* **2014**, *18*, 29–38.
- (40) Wolfenstine, J.; Rangasamy, E.; Allen, J. L.; Sakamoto, J. High Conductivity of Dense Tetragonal Li₇La₃Zr₂O₁₂. *J. Power Sources* **2012**, 208, 193–196.
- (41) Mayo, M. J. Processing of Nanocrystalline Ceramics from Ultrafine Particles. *Int. Mater. Rev.* **1996**, 41, 85–115.
- (42) Groza, J. R.; Dowding, R. J. Nanoparticulate Materials Densification. *Nanostruct. Mater.* **1996**, *7*, 749–768.
- (43) Fang, Z. Z.; Wang, H. Densification and Grain Growth during Sintering of Nanosized Particles. *Int. Mater. Rev.* **2008**, *53*, 326–352. (44) Lu, K. Sintering of Nanoceramics. *Int. Mater. Rev.* **2008**, *53*, 21–38.
- (45) Chen, I.-W.; Wang, X.-H. Sintering Dense Nanocrystalline Ceramics without Final-Stage Grain Growth. *Nature* **2000**, *404*, 168–171.
- (46) Zhang, G.; Kirk, B.; Jauregui, L. A.; Yang, H.; Xu, X.; Chen, Y. P.; Wu, Y. Rational Synthesis of Ultrathin N-Type Bi₂Te₃ Nanowires with Enhanced Thermoelectric Properties. *Nano Lett.* **2012**, *12*, 56–60.
- (47) Seabaugh, M. M.; Kerscht, I. H.; Messing, G. L. Texture Development by Templated Grain Growth in Liquid-Phase-Sintered Alpha-Alumina. *J. Am. Ceram. Soc.* **1997**, *80*, 1181–1188.
- (48) Kim, I.-D.; Rothschild, A.; Lee, B. H.; Kim, D. Y.; Jo, S. M.; Tuller, H. L. Ultrasensitive Chemiresistors Based on Electrospun TiO₂ Nanofibers. *Nano Lett.* **2006**, *6*, 2009–2013.
- (49) Hou, Y.-D.; Hou, L.; Zhao, J.-L.; Zhu, M.-K.; Yan, H. Lead-Free Bi-Based Complex Perovskite Nanowires: Sol-Gel-Hydrothermal Processing and the Densification Behavior. *J. Electroceram.* **2011**, *26*, 37–43.